

# Benchmarking an Even Better HEPTopTagger

Christoph Anders,<sup>1</sup> Catherine Bernaciak,<sup>2</sup> Gregor Kasieczka,<sup>3</sup> Tilman Plehn,<sup>2</sup> and Torben Schell<sup>2</sup>

<sup>1</sup>*Physikalisches Institut, Universität Heidelberg, Germany*

<sup>2</sup>*Institut für Theoretische Physik, Universität Heidelberg, Germany*

<sup>3</sup>*Institute for Particle Physics, ETH Zürich, Switzerland*

Top taggers are established analysis tools to reconstruct boosted hadronically decaying top quarks for example in searches for heavy resonances. We first present a dedicated study of signal efficiency versus background rejection, allowing for an improved choice of working points. Next, we determine to what degree our mass drop selection can be improved by systematically including angular correlations between subjects or N-Subjettiness. Finally, we extend the reach of the top tagger to transverse momenta below the top mass. This momentum range will be crucial in searches for the associated production of a Higgs boson with top quarks.

## Contents

<b>I. Introduction</b>	2
<b>II. The new default</b>	2
<b>III. Angular correlations</b>	6
<b>IV. N-Subjettiness</b>	7
<b>V. Low boost</b>	8
<b>VI. Outlook</b>	11
<b>References</b>	12

## I. INTRODUCTION

Because the top quark is the only observed fermion with a weak-scale mass it can be expected to have strong ties with the mechanism of electroweak symmetry breaking. Models which attempt to solve the hierarchy problem, like supersymmetry, top color, or little Higgs models [1], predict additional states in the top sector to ameliorate the effect of the top quark on the Higgs boson's mass. In the Higgs sector we can test modifications of the top Yukawa coupling in the associated production of a Higgs boson with a top pair [2–4]. An example for weakly interacting physics beyond the Standard Model, which modifies the top Yukawa coupling and can be used to complete the Standard Model with free Higgs couplings in the ultraviolet, is a two Higgs doublet model [5]. Typical signatures of new physics linked to the top sector include top partners decaying to top quarks and missing energy [6–8], heavy resonances decaying to two boosted tops [9, 10], or single top production [11].

The ultimate experimental goal at the LHC is to search for such effects in different decay channels, including the purely hadronic decay of two top quarks. In purely hadronic analyses we first have to overcome the multi-jet QCD background [12]. After that initial step we have to extract the signal out of top pair backgrounds, using the kinematics of the reconstructed tops. Recently, we have seen that the most promising phase space region for both of these two tasks are boosted top decays with  $p_{T,t} \gtrsim m_t$  [13]. Such a boost will, aside from other improvements, separate the decay products of two top quarks and offer an handle against combinatorial backgrounds [2, 12].

While hadronic signatures are the target of top taggers, experimental tests have to be performed with an event sample that can be easily controlled. Semi-leptonic top pairs can be triggered based on a hard lepton. The momentum of the lepton will also be strongly correlated with the transverse momentum of the hadronically decaying top quark. If necessary,  $b$ -tags can be used to control  $W$ +jets backgrounds. Because the aim of this paper is to improve the top tagging efficiency in particular towards lower transverse momenta we will present all of our findings in terms of semi-leptonic top pairs, so they can be easily reproduced by ATLAS and CMS.

The idea of studying the substructure of jets and using this structure to identify massive hadronically decaying particles has been around for almost 20 years [9, 14, 15]. In the following we will focus on tagging top quarks [2, 7, 16–21] with the help of the HEPTOPTAGGER and in a moderately boosted regime with  $p_{T,t} \lesssim 800$  GeV. In this framework ATLAS has published promising results [22], motivating this detailed study of top tagging in the upcoming 13 TeV run. To identify and reconstruct hadronic top decays with higher boost there exist specific HEPTOPTAGGER improvements [23]. Our study will be based on semi-leptonic top pair events which allows for relatively easy experimental tests in data.

As a first step we will introduce some minor modifications of the HEPTOPTAGGER algorithm in Section II. We will mostly target a possible shaping of QCD backgrounds towards an unphysical peak in the reconstructed top mass at low and high jet multiplicities. For this new default setup we will for the first time introduce receiver operating characteristics (ROC) curves to quantify the performance of the tagger beyond the known working points. In Section III we will extend the available observables in the tagging procedure by angular correlations, given in terms of Fox–Wolfram moments [24, 25]. In Section IV we will, in a similar spirit, test the combination of the HEPTOPTAGGER with  $N$ -Subjettiness. Finally, in Section V we will modify the tagging algorithm such that we can identify and reconstruct boosted tops down to  $p_{T,t} = 150$  GeV, as suggested by the MADMAX study of the  $t\bar{t}H$  process [26].

## II. THE NEW DEFAULT

In this first section we test two modifications of the HEPTOPTAGGER algorithm [7]. None of them will significantly change the performance of the tagger in terms of signal efficiency and background rejection. However, they are relevant for the reconstructed  $m_t^{\text{rec}}$  distribution for the QCD multi-jet background. Our signal event sample are semi-leptonic decays ( $\ell = e, \mu$ ) of  $t\bar{t}$  pairs with up to two additional matrix element jets, generated with ALPGEN [27] and PYTHIA [28] using MLM merging [29]. For the background we consider a leptonically decaying  $W$  plus 2 to 4 matrix element jets simulated the same way. On the generator level

$R_{\text{fat}}$	1.8	$R_{\text{min,max}}$	$(0.85 - 1.15) \times m_W/m_t$
$f_{\text{drop}}$	0.8	$m_{23}/m_{123}$ and $\arctan m_{13}/m_{12}$ cuts	0.35, 0.2, 1.3
$m_{\text{min}}$ [GeV]	30	$m_t^{\text{rec}}$ [GeV]	150-200
$N_{\text{filt}}$	5	$(m_W/m_t)^{\text{rec}}/(m_W/m_t)$	no cut

Table I: Parameters in the HEPTOPTAGGER algorithm, as defined in the text.

all hard jets have to fulfill  $p_{T,j} > 25$  GeV,  $|\eta_j| < 5$ , and  $\Delta R_{jj} > 0.4$ . The top mass used for simulation is 173 GeV. We initially study the current collider energy of  $\sqrt{s} = 8$  TeV and will then move to  $\sqrt{s} = 13$  TeV.

Throughout our analysis the top tagging algorithm operates on fat jets with the Cambridge–Aachen size  $R_{\text{fat}} = 1.8$ , reconstructed by FASTJET [30, 32]. In this section we require fat jets with  $p_{T,\text{fat}} > 200$  GeV and  $|\eta_{\text{fat}}| < 2.5$ . The increased size as compared to the old default of  $R_{\text{fat}} = 1.5$  will allow us to increase the tagging efficiency for moderate boost. This increase is triggered by the encouraging experimental studies of pile-up in filtered fat jets [31], but it might lead to a re-adjustment of the filtering parameters. For consistency reasons we only accept tagged tops with  $p_{T,\text{tag}} > 200$  GeV in this first step. We give all other tagging parameters in Table I: the mass drop required for a massive splitting is defined by  $\min m_{j_{1,2}}/m_j < f_{\text{drop}} = 0.8$ . The jet algorithm stops at subjets with  $m_{\text{min}} = 30$  GeV, where this parameter can be easily adapted to a more challenging detector environment. The  $W$  and top masses are defined on a filtered set of subjets allowing for  $N_{\text{filt}} = 5$  objects, *i.e.* including up to two jets from final state radiation. The kinematic conditions are parameterized by the HEPTOPTAGGER variables  $R_{\text{min,max}} = (0.85 - 1.15) \times m_W/m_t$ ,  $\arctan m_{13}/m_{12} = 0.2 - 1.3$ , and  $m_{23}/m_{123} > 0.35$ . The selected region has an  $A$ -like shape in the two dimensional plane [7]. Finally, the mass window of the reconstructed top mass is 150 – 200 GeV, while in the old default setup we do not apply a specific cut on the ratio of the reconstructed  $W$  and top masses.

Our first modification of the HEPTOPTAGGER algorithm affects the order in which we apply the top mass selection and the  $A$ -shaped  $W$  mass constraints. In the standard algorithm we early on select a filtered triplet of hard subjets closest to the top mass [7]. This triplet is then required to fulfill the different  $W$  and top mass cuts. The danger is that in the presence of more than one valid triplet of filtered subjets we pick the wrong one such that we are guaranteed not to pass the  $W$  mass constraints. To avoid this, we can first pre-select all triplets which pass the mass cuts and then pick the one with  $m_{123}$  closest to  $m_t$  out of those passing the  $W$  mass constraints. In Fig. 1 first see that both versions work on the signal events without an appreciable difference. The standard ordering slightly shapes the background around  $m_t \sim m_{123}$ .

The tagging efficiency and mis-tagging rates for both approaches applied to semi-leptonic top pairs are given in Table II. The signal efficiencies are defined as the number of tagged tops divided by the number of hadronically decaying tops in the event sample with  $p_{T,t} > 200$  GeV and  $|\eta_t| < 2.5$ . For the background we quote the number of mis-tags in the leptonic  $W$ +jets sample per number of fat jets passing  $p_{T,\text{fat}} > 200$  GeV and  $|\eta_{\text{fat}}| < 2.5$ . We see that with the new ordering both the signal efficiency and the background mis-tagging rate increase, such that typical significances stay constant. Based on the reduced shaping of the background mass distributions we will assume the new order of cuts as HEPTOPTAGGER standard.

If the algorithm described above is used in a high multiplicity environment, caused by multi-jet final states and contributions from pile-up, it is not guaranteed that there is a unique triplet of filtered subjets

		standard	inverted	$dj_{\text{sum}}$
		$ m_{123} - m_t $	$ m_{123} - m_t $	
8 TeV	$\varepsilon_S$	0.331	0.375	0.304
	$\varepsilon_B$	0.014	0.018	0.014
13 TeV	$\varepsilon_S$	0.337	0.394	0.305
	$\varepsilon_B$	0.015	0.021	0.016
		old default	new default	

Table II: (Mis)tagging efficiencies for standard and inverted cut order, in the latter case for the  $|m_{123} - m_t|$  and  $dj_{\text{sum}}$  selections. All cuts and tagging parameters are given in Table I. The new HEPTOPTAGGER default setting is indicated.

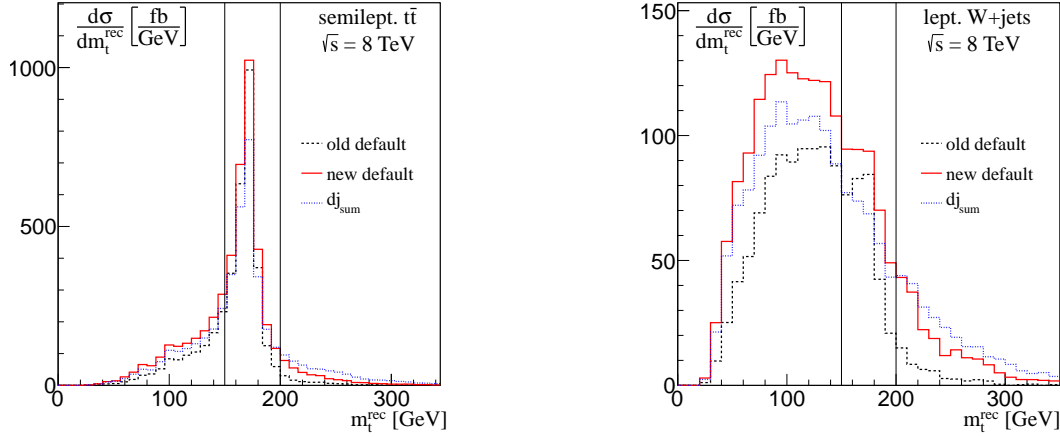


Figure 1: Reconstructed top mass for the signal (left) and background (right) samples at 8 TeV collider energy. We show the standard order of cuts with  $|m_{123} - m_t|$  selection (dashed black), the inverted order of cuts with  $|m_{123} - m_t|$  selection (solid red), and the inverted order of cuts with  $dj_{\text{sum}}$  selection (dotted blue).

which corresponds to the three top decay partons. The same problem arises for the Higgs tagger in the semileptonic boosted  $t\bar{t}H$  analysis. In that situation choosing the combination with  $|m_{12} - m_H|$  or in this case  $|m_{123} - m_t|$  is guaranteed to shape the background. To construct an alternative criterion for choosing the correct combination of subjects we start with the observation that the jet mass can be approximately linked to the Jade distance [33],

$$m_{ij}^2 \simeq E_i E_j \Omega_{ij}^2 \simeq p_{T,i} p_{T,j} (\Delta R_{ij})^2. \quad (1)$$

We can re-weight the transverse momenta and the geometric separation to construct an alternative metric for choosing subject combinations, like for example the modified Jade distance summed over the three top decay subject candidates,

$$dj_{\text{sum}} = \sum_{(ij)} d_{ij} \quad \text{with} \quad d_{ij} = p_{T,i} p_{T,j} (\Delta R_{ij})^4. \quad (2)$$

When we ask for the maximum modified Jade distance we enhance the weight of the geometric separation as compared to the jet mass, *i.e.* we prefer those subject combinations which are more widely separated. In Fig. 1 we compare the  $m_t^{\text{rec}}$  distributions with the old and new HEPTOPTAGGER default setups. For the signal as well as the background sample we find less candidates in the mass window 150 – 200 GeV. In addition, the background is even less shaped than for the inverted ordering described above. The corresponding (mis)tagging efficiencies are given in Table II. While we find a tiny improvement in the signal-to-background ratio compared to the new default setup, the signal efficiency is significantly reduced. We therefore include this new selection according to Eq.(2) as an option for high-multiplicity applications of the HEPTOPTAGGER, but do not make it the new default setting.

To conclusively test the performance of any algorithm, like the HEPTOPTAGGER, it is not sufficient to only study a single operating point like the one described in Table I. In particular to test possible improvements of the tagger [23] we need to study the correlation between the signal efficiency  $\varepsilon_S$  versus the background mis-identification probability  $\varepsilon_B$ . For the standard working point both of these efficiencies are described in Table II. The two-dimensional correlation of  $\varepsilon_S$  and  $1 - \varepsilon_B$  are described by a receiver operating characteristics (ROC) curve. Any point on this curve corresponds to an optimized parameter setting in the algorithm and can be chosen as the operating point for an analysis. We derive the ROC curves for the HEPTOPTAGGER using a boosted decision tree as implemented in TMVA [34]. In the TMVA analysis we vary the boundaries of the A-shaped constraints  $\arctan m_{13}/m_{12}$  and  $m_{23}/m_{123}$ . To avoid continuously re-running the algorithm

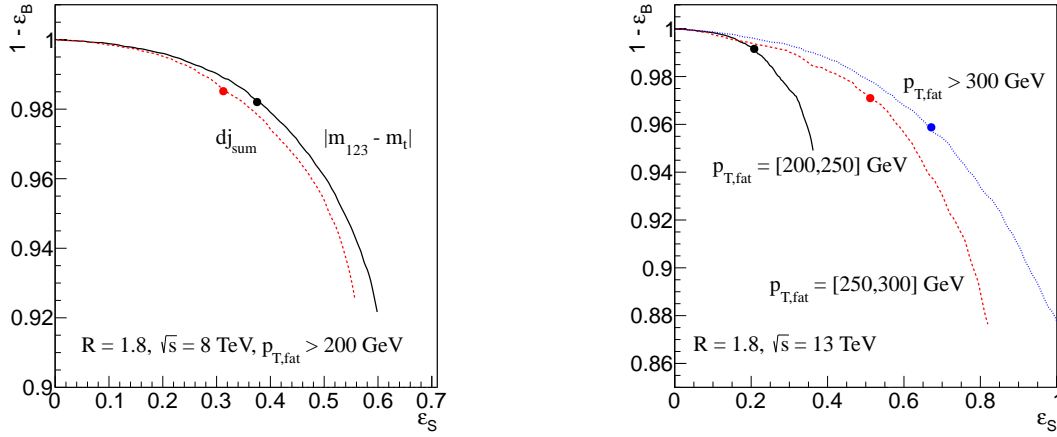


Figure 2: ROC curves for the modified HEPTOPTAGGER on semileptonic  $t\bar{t}$  pairs for 8 TeV (left) and 13 TeV (right) collider energy. The standard working points with the cuts given in Table I are indicated by dots. For 8 TeV we show the new default setup and the high-multiplicity modification. For 13 TeV we quote the performance in slices of  $p_{T,\text{fat}}$ .

we only allow for tighter cuts than the default algorithm. The top mass window which is not part of the actual fat jet algorithm can change without external constraint, and we include an additional cut on the reconstructed mass ratio  $(m_W/m_t)^{\text{rec}}$ . For more details on the BDT optimization we refer to Ref. [25].

In the left panel of Fig. 2 we show ROC curves for the re-ordered HEPTOPTAGGER algorithm for 8 TeV collider energy. We show results for the new standard setup and the high-luminosity setup ordered by the modified Jade distance of Eq.(2). As mentioned before, the efficiency for the signal is defined as the number of tagged tops normalized to the number of hadronically decaying tops with  $p_{T,t} > 200$  GeV and  $|\eta_t| < 2.5$ . For the background the normalization is given by the number of fat jets fulfilling the same  $p_T$  and  $\eta$  criteria. Computed for the full  $t\bar{t}$  sample we reach signal efficiencies of 40% for a background rejection over 97.5%. When computed over the entire  $p_T$  range of the fat jet or top quark we see that the algorithm essentially breaks down at signal efficiencies above  $\varepsilon_S = 0.6$ . The reason is that the number of possibly tagged tops is limited by the number of tops with all three decay subjets inside the fat jet.

For 13 TeV, shown in the right panel of Fig. 2, we break the efficiency into three transverse momentum slices of the top or the fat jets, namely  $p_T = 200 - 250$  GeV,  $p_T = 250 - 300$  GeV, and  $p_T > 300$  GeV. Higher transverse momenta will be statistically limited in the  $t\bar{t}$  sample and are not the focus of this study. The signal efficiencies are defined as the number of tags obtained from the considered fat jets divided by the number of hadronically decaying tops in the event sample within the given range of transverse momenta. The combined curve for the  $t\bar{t}$  sample will essentially coincide with the lowest  $p_T$  bin, simply because of the composition of the signal events. Again, we observe that the signal efficiency is limited in the soft region. Above  $p_{T,t} = 300$  GeV we can reach almost 100% signal efficiencies. The performance of the new default working point from Table I is indicated by a dot. Depending on the analysis, we see that over the entire  $p_T$  range the HEPTOPTAGGER can reach a QCD background rejection of 99% for signal efficiencies between 20% for soft tops and 40% for hard tops. If required, the optimal working point of the top tagger can be chosen as a function of the fat jet momentum for example to guarantee a constant signal efficiency or background rejection according to Fig. 2.

The one remaining question is if the new version of the HEPTOPTAGGER still benefits from the pruned reconstructed top mass [18], as it does for the old version [23]. In terms of the ROC curves shown in Fig. 2 we can compare the new default tagger with the version including the pruned mass. It turns out that the two ROC curves are identical for each transverse momentum slice. The former improvement based on including the pruned mass is already taken into account in the improved efficiencies shown in Table II.

### III. ANGULAR CORRELATIONS

To make a conclusive statement about possible improvements to the HEPTOPTAGGER by using angular correlations of the subjets we need a systematic way to include such angular correlations. Correlations between a pair of subjets or other objects can be fully described in the basis of spherical harmonics. Fox–Wolfram moments are then constructed as a sum over all  $2\ell + 1$  directions, weighted by a free function  $W_i$  [24]

$$H_\ell^x = \frac{4\pi}{2\ell+1} \sum_{m=-\ell}^{\ell} \left| \sum_{i=1}^N W_i^x Y_\ell^m(\Omega_i) \right|^2. \quad (3)$$

The index  $i$  runs over all  $N$  objects. The individual coordinates  $\Omega_i$  can be replaced by the corresponding angular separation  $\Omega_{ij}$ , allowing us to write the moments in terms of Legendre polynomials

$$H_\ell^x = \sum_{i,j=1}^N W_{ij}^x P_\ell(\cos \Omega_{ij}) \quad \text{with} \quad W_{ij}^x = W_i^x W_j^x. \quad (4)$$

Two common weights are the transverse momentum or the unit weights [24, 25]

$$W_{ij}^T = \frac{p_{Ti} p_{Tj}}{(\sum p_{Ti})^2} \quad W_{ij}^U = \frac{1}{N^2}. \quad (5)$$

The advantage of the transverse-momentum weight is that it suppresses soft and collinear jets, which are hard to correctly describe in QCD. However, tests show us that inside a top tagger the unit weight is more promising. Therefore, we do not use the transverse momentum weight in this analysis. We could in principle also compute these moments over other objects inside the fat jet, for example before filtering or the five subjet structures before re-clustering. However, all of this would make our results process dependent and hence not suitable for this study.

Using the unit weight the Fox–Wolfram moments analyze the angular correlations inside the fat jet. We evaluate them in the top rest frame, to remove the leading effect from the boost. This means that for the unit weights we do not have to define a reference axis and only two of the three angles between the subjets are independent. The fourth direction is given by the direction of the fat jet or the boost into the top rest frame.

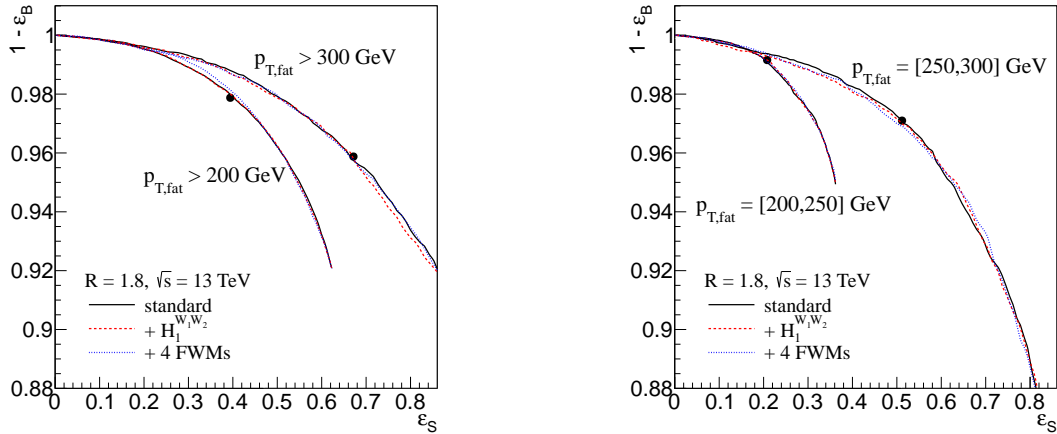


Figure 3: ROC curves for the modified HEPTOPTAGGER including angular correlations via unit-weight Fox–Wolfram moments in slices of  $p_{T,fat}$ . The standard working point from Table I is indicated by a dot. We assume a collider energy of 13 TeV.

To quantify the improvement which can be gained from the angular correlation we evaluate the Fox–Wolfram moments for each combination of subjets using a boosted decision tree as implemented in TMVA. For the angular analysis we label the two subjets which reconstruct  $m_W$  best as  $W_1$  and  $W_2$ , ordered by transverse momentum. The remaining subjet is then labeled the  $b$ -jet. As long as we include a full set of correlations in the Fox–Wolfram moments, these names do not matter for the performance. They will only become relevant once we interpret the results. Using TMVA we determine the most decisive moments for each combination of two to four subjets and the boost direction, *i.e.* two spatial directions out of  $\{W_1, W_2, b, \vec{p}_{\text{boost}}\}$ . This allows us to define a limited set of Fox–Wolfram moments which we can reliably compare to the purely kinematics–based selection discussed before.

In Fig. 3 we show ROC curves for the full event sample and for slices in the transverse momentum of the fat jet. The purely QCD-inspired selection criteria of Table I is contrasted with the selection including the available angular correlations. The moment with the strongest separation for signal and background is the first moment  $H_1^U$  built from the two  $W$  decay jets. However, for all four  $p_{T,\text{fat}}$  choices we see that including this additional information has no effect on the performance of the tagger.

In addition, we show results including the leading moments from the best sets of momenta. As mentioned above, the leading moment is  $H_1^U$  from the  $(W_1, W_2)$  selection. Other examples for highly ranked moments are  $H_2^U$  from the  $(W_1, W_2, \vec{p}_{\text{boost}})$  selection or  $H_1^U$  defined over  $(W_2, b, \vec{p}_{\text{boost}})$ . The results from an optimized tagger using the best four moments are also shown in Fig. 3, again with no visible improvement.

The bottom line of this systematic analysis of angular correlations in top tagger is that the angular correlations among the top decay products and the top direction are already included in the QCD–based selection. Apparent improvements are within the reach of the ROC curve. For the given transverse momentum range adding more angular information does not lead to a measurable improvement of the HEPTOPTAGGER.

#### IV. N-SUBJETTINESS

A second way to identify boosted hadronically decayed top quarks could be a combination of a mass-drop criterion with  $N$ -Subjettiness [35]. This additional observable measures how well a fat jet is described by a given number of subjets. It starts by constructing  $N$  reference axes and then measures how well the  $k$  fat jet constituents fit to those axes,

$$\tau_N = \frac{1}{R_0 \sum_k p_{T,k}} \sum_k p_{T,k} \min(\Delta R_{1,k}, \Delta R_{2,k}, \dots, \Delta R_{N,k}) . \quad (6)$$

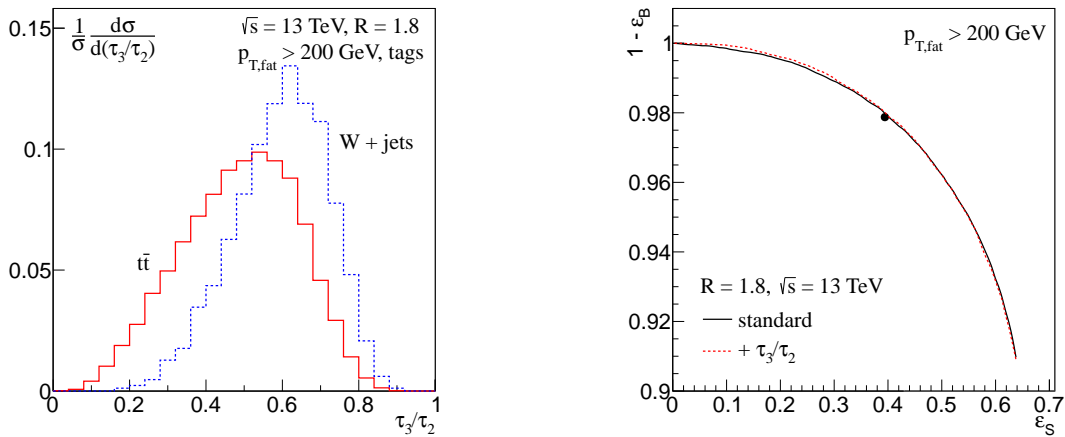


Figure 4: Left:  $\tau_3/\tau_2$  for tagged fat jets. The red solid curves show the  $t\bar{t}$  signal while the blue dotted curves give the  $W$ +jets background. Right: ROC curves for the combined HEPTOPTAGGER and  $\tau_3/\tau_2$ .

$\Delta R$  is the usual geometric separation and  $R_0$  is an intrinsic cone size, usually the value used to construct the fat jet. Small values of  $\tau_N$  indicate that the jet is consistent with fewer than  $N$  subjets. Consequently, ratios of the kind  $\tau_N/\tau_{N-1}$  allow us to distinguish between jets described by  $N$  or  $N-1$  substructures. For top tagging the ratio  $\tau_3/\tau_2$  is expected to be most useful.

Similar to the case of angular correlations studied in the previous section, we combine the HEPTOPTAGGER [7] setup given in Table I with  $N$ -Subjettiness based on axes using the one-pass- $k_T$  method implemented in SPARTYJET [36].

In the left panel of Fig. 4 we show the  $\tau_3/\tau_2$  distributions for the fat jets tagged by the new default HEPTOPTAGGER. We see that  $\tau_3/\tau_2$  without any additional cuts carries information that can be used to distinguish between signal and background. To check the power of this additional variable in addition to the tagging algorithm we again compute the corresponding ROC curve with a variable combination of tagging parameters and  $N$ -Subjettiness using boosted decision trees as implemented in TMVA [34]. We show the results in the right panel of Fig. 4: first, we show the new default HEPTOPTAGGER described in Section II, allowing for an optimized mass window  $m_{123}$  as well as tighter  $A$ -shaped mass plane cuts and a cut on  $m_W/m_t$ . We then include  $\tau_3/\tau_2$  in the boosted decision tree and see that it gives a hardly visible improvement in the low efficiency range.

The bottom line of this analysis of a combined mass-drop and  $N$ -Subjettiness tagger is again that the additional information includes relevant information, but that it does not lead to an improvement compared to an optimized HEPTOPTAGGER setup. The apparent improvement corresponds merely to a shift in the working point of the mass drop tagger.

## V. LOW BOOST

The lesson we learned in Sections III and IV, namely that adding angular correlations or additional observables to the tagging algorithm has essentially no effect, is limited to sufficiently boosted top quarks for which the algorithm has the chance to identify all three decay jets from mass drop criteria. In the range of  $p_{T,t} = 150 - 200$  GeV this might not be the case, while the fat jet still includes most of the kinematic information from the top decay. For example, the softest decay jet might be pushed outside the fat jet and replaced by an initial state QCD jet, but the two leading jets could still be used to identify a massive top decay. For such events the mass drop criterion will not be efficient enough to separate the signal from the background, which brings us back to angular correlations between the decay products.

One obvious application for a top tagger at low momenta is the associated production of a Higgs with a pair of top quarks [2]. In Table III we show the fraction of events for this process including one or two top quarks with  $p_{T,t} > 150$  GeV or  $p_{T,t} > 200$  GeV. Reducing the transverse momentum threshold by 50 GeV increases the number of events by 50% for one top tag and by 100% for two top tags.

The default HEPTOPTAGGER has never targeted top quarks with  $p_{T,t} < 200$  GeV. This consistency condition is related to the size of the fat jet and based on the assumption that the algorithm has to be able to see all three top decay subjets [7]. In this section we suggest a new analysis step targeting events with  $p_{T,t}^{\text{rec}} = 150 - 200$  GeV. In this range we will employ angular correlations through the Fox–Wolfram moments, introduced in the last section.

$\sigma_{\text{tot}} = 360 \text{ fb}$	all $p_{T,H}$	$p_{T,H} > 100 \text{ GeV}$
all $p_{T,t}$	100%	48%
$p_{T,t_1} > 150 \text{ GeV}$	59%	37%
$p_{T,t_1} > 200 \text{ GeV}$	39%	27%
$p_{T,t} > 150 \text{ GeV}$	29%	16%
$p_{T,t} > 200 \text{ GeV}$	15%	8.8%

Table III: Fraction of the total cross section for  $t\bar{t}H$  production at 13 TeV, passing a range of cuts on the transverse momentum of the harder top ( $p_{T,t_1}$ ) or both tops ( $p_{T,t}$ ).

	default		low- $p_T$ mode	
	(mis)tags [fb]	fraction	(mis)tags [fb]	fraction
type-1	5309	57%	5967	52%
type-2	1283	14%	1863	16%
type-3	2712	29%	3601	32%
$\varepsilon_S$	0.287		0.353	
$W$ +jets	1200		1663	
$\varepsilon_B$	0.007		0.010	

Table IV: Comparison of tagging results in the new default setup without (left) and with the low- $p_T$  mode (right). All tags fulfill  $p_{T,\text{fat}} > 150$  GeV as well as  $p_{T,\text{tag}} = 150 - 200$  GeV. The working point for the low- $p_T$  mode is given in Table V. The quoted cross section values correspond to the semi-leptonic  $t\bar{t}$  sample.

As before, our study is based on semi-leptonically decaying top pairs. The size of the fat Cambridge–Aachen jet is  $R_{\text{fat}} = 1.8$ , and it is required to have  $p_{T,\text{fat}} > 150$  GeV and  $|\eta_{\text{fat}}| < 2.5$ . Those fat jets are analyzed with the (new) default HEPTOPTAGGER described in Section II. To determine the quality of each top tag with  $p_{T,t}^{\text{rec}} = 150 - 200$  GeV we rely on the geometric separation of the parton-level top decay jets and the reconstructed top constituents for a given mapping  $j_i$  [23],

$$\Delta R_{\text{sum}}^2 = \sum_{i=1}^3 \Delta R^2(p_i^{\text{rec}}, p_{j_i}^{\text{parton}}) . \quad (7)$$

We minimize  $\Delta R_{\text{sum}}^2$  to define the best mapping of parton level and reconstructed top decay products. Based on the parton level information we can then assign it to one of three types:

- type-1: all three subjets of the tagged top quark correspond to top decay products at parton level,
- type-2: the two hardest subjets correspond to top decay products, the third subjet does not,
- type-3: everything else.

This way the type-3 category includes events where one or zero subjets correspond to top decay products, but also events where only the hardest subjet cannot be assigned to a top decay parton. In Table IV we see the fraction of type-1 to type-3 tags after requiring a reduced threshold  $p_{T,\text{fat}} > 150$  GeV and only considering a low- $p_T$  slice with  $p_{T,t}^{\text{rec}} = 150 - 200$  GeV. For the default tagger with these two modifications 57% of the additional tags are of type-1, *i.e.* all top decay products can be assigned to parton level information. For an additional 14% of events the two leading subjets can be linked to top decay product at parton level, while for 29% this matching is problematic.

The critical step at which not perfectly matched top decays in the type-2 and type-3 categories fail the default tagging algorithm is the final mass window  $m_t^{\text{rec}} = 150 - 200$  GeV. In the modified low- $p_T$  mode the HEPTOPTAGGER first accepts all tagged tops with  $m_t^{\text{rec}} = 150 - 200$  GeV, as long as they fulfill the now lower consistency criterion  $p_{T,\text{tag}} = 150 - 200$  GeV.

	min	max
$m_t^{\text{rec}}$ [GeV]	108.	282.
$(m_W/m_t)^{\text{rec}}/(m_W/m_t)$	0.717	1.556
$\arctan(m_{13}/m_{12})$	0.441	0.889
$m_{23}/m_{123}$	0.412	0.758
$H_1^{W_1 W_2}$	0.048	0.373
$H_2^{p W_1 W_2}$	0.019	0.524
$H_2^{p b W_1 W_2}$	0.044	0.276
$H_1^{p b W_2}$	0.145	0.445

Table V: Cuts defining the working point used for the low- $p_T$  mode shown in Fig. IV. The values are extracted using simulated annealing.

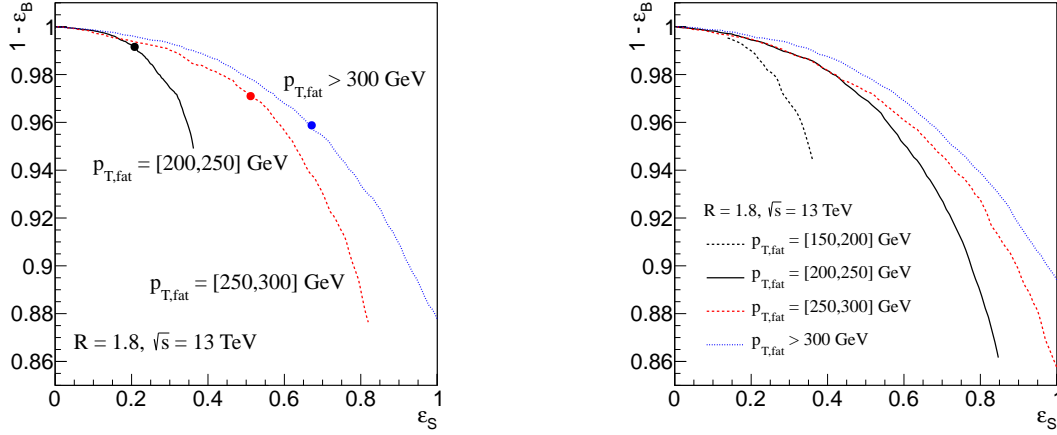


Figure 5: ROC curves for the new standard HEPTOPTAGGER without (left) and with the new low- $p_T$  mode (right) in slices of  $p_{T,\text{fat}}$ . The signal performance is given for semileptonic  $t\bar{t}$  pairs at 13 TeV collider energy.

We then target all events which do not pass the  $m_t^{\text{rec}}$  condition but fall within the transverse momentum range  $p_{T,\text{tag}} = 150 - 200$  GeV. For them we widen the  $m_t^{\text{rec}}$  window and add a new requirement for the reconstructed  $W$  to top mass ratio. In Table V we quote one working point for illustration purposes. Two cuts on  $\arctan(m_{13}/m_{12})$  and  $m_{23}/m_{123}$  are part of the  $A$ -shaped selection in the original tagging algorithm, which means all events passing the tagging algorithm lie inside this  $A$ -shape. Just as in the ROC analysis of Section II we now allow for an additional cut on both of these subjet observables. Finally, we include the best Fox-Wolfram moments in the four leading jet selections. The cut values quoted in Table V define one working point on the ROC curve for the low- $p_T$  mode. The corresponding efficiencies for this point are quoted in Table IV. Its efficiency over the  $t\bar{t}$  sample with a hadronically decaying top in the same  $p_T$  range is significantly increased from 29% to 35%, with a slightly larger fraction of type-2 and type-3 events. In many applications of the top tagger these low- $p_T$  top decays constitute most of the signal sample, as shown for the  $t\bar{t}H$  production process in Table III. Here, the low- $p_T$  improvement might increase the over-all number of tagged signal events by up to 20%.

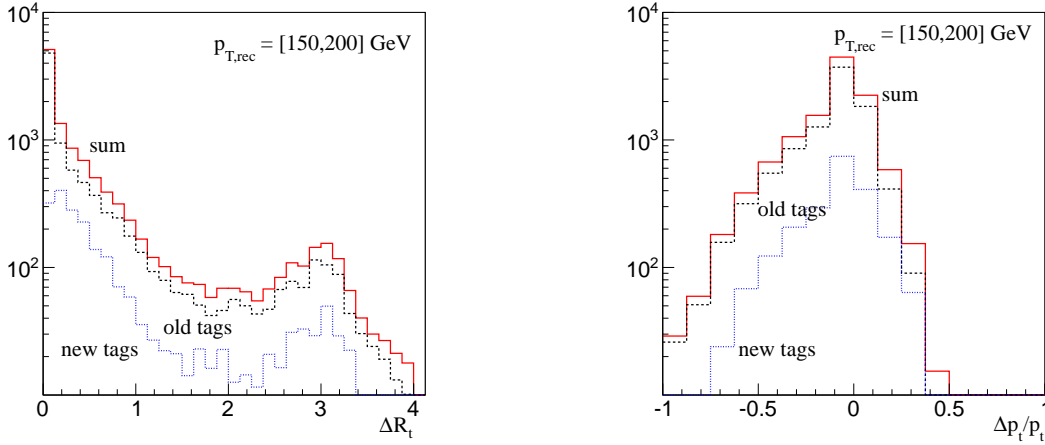


Figure 6: Reconstruction for the original tags (black), the additional tags in the low- $p_T$  mode (blue), and all events in the semi-leptonic  $t\bar{t}$  sample (red). We show the angular difference and the relative difference in transverse momentum between the reconstructed top momentum and parton level truth for all tagged tops.

To compute an ROC curve for the low- $p_T$  mode we optimize the tagging parameters only for type-2 tags which did not pass the original algorithm. According to Table IV optimizing on all events would give a significant weight to type-3 events, which would lead to an increased number of tags with very poor top reconstruction. We therefore compute the ROC curve of the low- $p_T$  tagger by optimizing the tagger for type-2 events in the  $p_{T,\text{fat}} = 150 - 200$  GeV band. We then compute the corresponding efficiencies for the entire  $t\bar{t}$  sample. In Fig. 5 we compare the performance of the low- $p_T$  mode to the new default tagger shown in Fig. 2. We see first of all that the new mode makes the slice with  $p_{T,\text{fat}} = 150 - 200$  GeV competitive with the softest slice in the standard setup. Also the slice with fat jets within  $p_{T,\text{fat}} = 200 - 250$  GeV benefits from the new mode, because a large number of newly tagged events with  $p_{T,t}^{\text{rec}} = 150 - 200$  GeV appear in that slice. As mentioned above, in the new version the cuts and tagging criteria can be optimized depending on the transverse momentum for example of the fat jet, to improve a given analysis.

Before we can make use of the significant improvement documented above, we need to ensure that for the tops tagged in the low- $p_T$  mode the HEPTOPTAGGER reconstructs the direction and the 4-momentum as well as for the original setup. In Fig. 6 we see that the dedicated low- $p_T$  tags inside the HEPTOPTAGGER have almost the same quality of the standard tags in the same transverse momentum range [23]. We show the geometric distance  $\Delta R_t$  between the reconstructed top momentum and the parton level top momentum as well as the normalized deviation in transverse momentum,  $\Delta p_t/p_t = (p_{T,t}^{\text{rec}} - p_{T,t}^{\text{true}})/p_{T,t}^{\text{rec}}$ . The only slight weakness of the low- $p_T$  mode is the depleted region with excellent angular resolution, *i.e.*  $\Delta R_t \lesssim 0.1 \ll R_{\text{fat}} = 1.8$ . We actually expect that this precision can be improved by a dedicated calibration procedure, which is beyond the capabilities of the kind of study we present here.

## VI. OUTLOOK

In this top tagging study we defined the new default setup of the HEPTOPTAGGER for the upcoming 13 TeV run, with a focus on moderate boosts of  $p_{T,t} > 150$  GeV. The entire study is based on the experimentally accessible semi-leptonic  $t\bar{t}$  sample. Our key results are

1. For large fat jets with  $R_{\text{fat}} = 1.8$  we define a new default setup with reduced shaping of the multi-jet background. In addition, we provide a specific high-multiplicity mode for the tagger.
2. We give ROC curves which allow us to define the most appropriate working points depending on the transverse momentum of the fat jet. An optimal working point can be chosen for individual analyses, including  $p_T$ -dependent parameter choices.
3. Including angular correlations after the QCD-inspired selection does not improve the tagging performance for  $p_{T,\text{fat}} > 200$  GeV. The same is true for the pruned mass as an additional observable. The QCD-inspired tagging algorithm appears to be highly efficient in extracting the available information.
4. Similarly, combining the HEPTopTagger with  $N$ -Subjettiness does not give significant improvement in terms of the ROC curve.
5. We define a low- $p_T$  mode probing tops down to  $p_{T,t} = 150$  GeV, which makes use of angular correlations for tops with only part of their decay products captured inside the fat jet. For the  $t\bar{t}$  sample this leads to a the signal efficiency of 35% in the targeted momentum range.

With those modifications we expect the HEPTOPTAGGER to be even more useful for a wide range of analyses to come, including  $t\bar{t}H$  searches.

## Acknowledgments

All of us would like to thank Sebastian Schätzel for his key contributions which made the HEPTOPTAGGER an experimental success.

- 
- [1] D. E. Morrissey, T. Plehn and T. M. P. Tait, Phys. Rept. **515**, 1 (2012).
  - [2] T. Plehn, G. P. Salam and M. Spannowsky, Phys. Rev. Lett. **104**, 111801 (2010).
  - [3] for a nice description of the experimental challenges see J. Cammin and M. Schumacher, ATL-PHYS-2003-024.
  - [4] see *e.g.* T. Plehn and M. Rauch, Europhys. Lett. **100**, 11002 (2012).
  - [5] see *e.g.* D. Lopez-Val, T. Plehn and M. Rauch, JHEP **1310**, 134 (2013).
  - [6] P. Meade and M. Reece, Phys. Rev. D **74**, 015010 (2006); J. Ellis, F. Moortgat, G. Moortgat-Pick, J. M. Smillie and J. Tattersall, Eur. Phys. J. C **60**, 633 (2009); K. Rolbiecki, J. Tattersall and G. Moortgat-Pick, Eur. Phys. J. C **71**, 1517 (2011); M. Perelstein and A. Weiler, JHEP **0903**, 141 (2009).
  - [7] T. Plehn, M. Spannowsky, M. Takeuchi, and D. Zerwas, JHEP **1010**, 078 (2010); <http://www.thphys.uni-heidelberg.de/~plehn/>
  - [8] K. Rehermann and B. Tweedie, JHEP **1103**, 059 (2011); T. Plehn, M. Spannowsky, M. Takeuchi, JHEP **1105**, 135 (2011).
  - [9] W. Skiba and D. Tucker-Smith, Phys. Rev. D **75**, 115010 (2007); B. Holdom, JHEP **0703**, 063 (2007). M. Gerbush, T. J. Khoo, D. J. Phalen, A. Pierce and D. Tucker-Smith, Phys. Rev. D **77**, 095003 (2008); G. Brooijmans, ATL-PHYS-CONF-2008-008 and ATL-COM-PHYS-2008-001, Feb. 2008.
  - [10] see *e.g.* K. Agashe, A. Belyaev, T. Krupovnickas, G. Perez and J. Virzi, Phys. Rev. D **77**, 015003 (2008) V. Barger, T. Han and D. G. E. Walker, Phys. Rev. Lett. **100**, 031801 (2008); B. Lillie, L. Randall and L. -T. Wang, JHEP **0709**, 074 (2007); U. Baur and L. H. Orr, Phys. Rev. D **76**, 094012 (2007); U. Baur and L. H. Orr, Phys. Rev. D **77**, 114001 (2008); P. Fileviez Perez, R. Gavin, T. McElmurry and F. Petriello, Phys. Rev. D **78**, 115017 (2008).
  - [11] F. Kling, T. Plehn and M. Takeuchi, Phys. Rev. D **86**, 094029 (2012).
  - [12] M. R. Buckley, T. Plehn and M. Takeuchi, JHEP **1308**, 086 (2013); M. R. Buckley, T. Plehn, T. Schell and M. Takeuchi, arXiv:1310.6034 [hep-ph].
  - [13] A. Abdesselam *et al.*, Eur. Phys. J. C **71**, 1661 (2011); T. Plehn and M. Spannowsky, J. Phys. G **39**, 083001 (2012); A. Altheimer *et al.*, arXiv:1311.2708 [hep-ex].
  - [14] M. H. Seymour, Z. Phys. C **62**, 127 (1994); J. M. Butterworth, B. E. Cox and J. R. Forshaw, Phys. Rev. D **65**, 096014 (2002).
  - [15] J. M. Butterworth, A. R. Davison, M. Rubin and G. P. Salam, Phys. Rev. Lett. **100**, 242001 (2008).
  - [16] D. E. Kaplan, K. Rehermann, M. D. Schwartz and B. Tweedie, Phys. Rev. Lett. **101**, 142001 (2008).
  - [17] L. G. Almeida, S. J. Lee, G. Perez, I. Sung and J. Virzi, Phys. Rev. D **79**, 074012 (2009); L. G. Almeida, S. J. Lee, G. Perez, G. F. Sterman, I. Sung and J. Virzi, Phys. Rev. D **79**, 074017 (2009); L. G. Almeida, S. J. Lee, G. Perez, G. Sterman, I. Sung, Phys. Rev. D **82**, 054034 (2010).
  - [18] S. D. Ellis, C. K. Vermilion and J. R. Walsh, Phys. Rev. D **80**, 051501 (2009); S. D. Ellis, C. K. Vermilion and J. R. Walsh, Phys. Rev. D **81**, 094023 (2010); C. K. Vermilion, arXiv:1101.1335 [hep-ph].
  - [19] J. Thaler, L. -T. Wang, JHEP **0807**, 092 (2008); D. Krohn, J. Thaler and L. -T. Wang, JHEP **0906**, 059 (2009); D. Krohn, J. Thaler, L. -T. Wang, JHEP **1002**, 084 (2010).
  - [20] J. Thaler, K. Van Tilburg, JHEP **1103**, 015 (2011); J. Thaler and K. Van Tilburg, JHEP **1202**, 093 (2012).
  - [21] A. Hook, M. Jankowiak and J. G. Wacker, JHEP **1204**, 007 (2012); M. Jankowiak and A. J. Larkoski, JHEP **1106**, 057 (2011); M. Jankowiak and A. J. Larkoski, JHEP **1204**, 039 (2012); D. E. Soper and M. Spannowsky, Phys. Rev. D **87**, no. 5, 054012 (2013); S. Schaetzel and M. Spannowsky, arXiv:1308.0540 [hep-ph].
  - [22] ATLAS Collaboration, JHEP **1301**, 116 (2013); ATLAS Collaboration, ATLAS-CONF-2013-084; G Piacquadio CERN-THESIS-2010-027; G Kasieczka, PhD thesis, <http://www.ub.uni-heidelberg.de/archiv/14941>.
  - [23] T. Plehn, M. Spannowsky and M. Takeuchi, Phys. Rev. D **85**, 034029 (2012).
  - [24] G. C. Fox and S. Wolfram, Phys. Rev. Lett. **41**, 1581 (1978); R. D. Field, Y. Kanev and M. Tayebnejad, Phys. Rev. D **55**, 5685 (1997).
  - [25] C. Bernaciak, M. S. A. Buschmann, A. Butter and T. Plehn, Phys. Rev. D **87**, 073014 (2013); C. Bernaciak, B. Mellado, T. Plehn, X. Ruan, and P. Schichtel, arXiv:1311.5891 [hep-ph].
  - [26] T. Plehn, P. Schichtel and D. Wiegand, arXiv:1311.2591 [hep-ph].
  - [27] M. L. Mangano, M. Moretti, F. Piccinini, R. Pittau and A. D. Polosa, JHEP **0307**, 001 (2003).
  - [28] T. Sjostrand, S. Mrenna and P. Z. Skands, JHEP **0605**, 026 (2006).
  - [29] M. L. Mangano, M. Moretti, R. Pittau, Nucl. Phys. B **632**, 343-362 (2002).
  - [30] Y. L. Dokshitzer, G. D. Leder, S. Moretti and B. R. Webber, JHEP **9708**, 001 (1997); M. Wobisch and T. Wengler, arXiv:hep-ph/9907280.
  - [31] ATLAS Collaboration, JHEP **1309**, 076 (2013).
  - [32] M. Cacciari and G. P. Salam, Phys. Lett. B **641**, 57 (2006); M. Cacciari, G. P. Salam and G. Soyez, Eur. Phys. J. C **72**, 1896 (2012); <http://fastjet.fr>
  - [33] W. Bartel *et al.* [JADE Collaboration], Z. Phys. C **33**, 23 (1986).
  - [34] A. Höcker *et al.*, PoS ACAT , 040 (2007) [physics/0703039 [PHYSICS]]; P. Speckmayer, A. Höcker, J. Stelzer and

H. Voss, J. Phys. Conf. Ser. **219**, 032057 (2010); <http://tmva.sourceforge.net>

- [35] J. Thaler and K. Van Tilburg, JHEP **1103**, 015 (2011); J. Thaler and K. Van Tilburg, JHEP **1202**, 093 (2012);  
I. W. Stewart, F. J. Tackmann and W. J. Waalewijn, Phys. Rev. Lett. **105**, 092002 (2010).
- [36] P. -A. Delsart, K. L. Geerlings, J. Huston, B. T. Martin and C. K. Vermilion, arXiv:1201.3617 [hep-ex].